Cancer Research

miR-193b–Regulated Signaling Networks Serve as Tumor Suppressors in Liposarcoma and Promote Adipogenesis in Adipose-Derived Stem Cells

Ying Z. Mazzu[1], Yulan Hu[1], Rajesh K. Soni[2], Kelly M. Mojica[1], Li-Xuan Qin[3], Phaedra Agius[4], Zachary M. Waxman[1], Aleksandra Mihailovic[5], Nicholas D. Socci[4], Ronald C. Hendrickson[2], Thomas Tuschl[5], and Samuel Singer[1]

Abstract

Well-differentiated and dedifferentiated liposarcomas (WDLS/DDLS) account for approximately 13% of all soft tissue sarcoma in adults and cause substantial morbidity or mortality in the majority of patients. In this study, we evaluated the functions of miRNA (miR-193b) in liposarcoma *in vitro* and *in vivo*. Deep RNA sequencing on 93 WDLS, 145 DDLS, and 12 normal fat samples demonstrated that miR-193b was significantly underexpressed in DDLS compared with normal fat. Reintroduction of miR-193b induced apoptosis in liposarcoma cells and promoted adipogenesis in human adipose-derived stem cells (ASC). Integrative transcriptomic and proteomic analysis of miR-193b–target networks identified novel direct targets, including CRK-like proto-oncogene (CRKL) and focal adhesion kinase (FAK). miR-193b was found to regulate FAK–SRC–CRKL signaling through CRKL and FAK. miR-193b also stimulated reactive oxygen species signaling by targeting the antioxidant methionine sulfoxide reductase A to modulate liposarcoma cell survival and ASC differentiation state. Expression of miR-193b in liposarcoma cells was downregulated by promoter methylation, resulting at least in part from increased expression of the DNA methyltransferase DNMT1 in WDLS/DDLS. *In vivo*, miR-193b mimetics and FAK inhibitor (PF-562271) each inhibited liposarcoma xenograft growth. In summary, miR-193b not only functions as a tumor suppressor in liposarcoma but also promotes adipogenesis in ASC. Furthermore, this study reveals key tyrosine kinase and DNA methylation pathways in liposarcoma, some with immediate implications for therapeutic exploration. *Cancer Res; 77(21); 5728–40. ©2017 AACR.*

Introduction

Liposarcomas account for about 20% of adult sarcomas (1, 2). Well-differentiated liposarcomas (WDLS) and dedifferentiated liposarcomas (DDLS), characterized by chromosome 12q13–15 amplification, represent the most common biologic group of liposarcoma (3). Primary WDLS, a low-grade disease, can evolve to DDLS, the high-grade form. Despite complete surgical resection, over 60% of patients with retroperitoneal WDLS and DDLS eventually have recurrence and die of disease (4). Once advanced disease develops and surgery is no longer possible, conventional chemotherapy is largely palliative with few long-term responses (5). Therefore, there is pressing need to understand the molecular alterations that drive the development and progression of liposarcoma so as to identify promising therapeutic targets.

Small noncoding RNAs (miRNA) play major roles in almost all biological pathways in mammals, and they are predicted to regulate more than 60% of all mRNAs (6). The importance of miRNAs in cancer has been demonstrated by the identification of dysregulated miRNA expression and through functional characterization of miRNA target networks (7). miRNAs not only have potential to serve as biomarkers of clinical outcome, but also represent an entry point for the discovery of dysregulated pathways in cancer and for identification of promising therapeutic targets.

Although miRNAs have been extensively investigated in many cancers, there is still limited insight into miRNA functions in liposarcoma. Several studies report dysregulation of miRNAs in liposarcoma (8–10), but only a few miRNAs have been demonstrated to be functional (8–13). In this study, we describe the results of miRNA sequencing analysis of tumors from a large cohort of patients with WDLS and DDLS. We discovered that miR-193b functions as a novel tumor suppressor in liposarcoma. A combination of computational, gene ontology, and functional analyses revealed pivotal roles of miR-193b–regulated FAK–SRC–CRKL signaling and reactive oxygen species (ROS) signaling in both liposarcomagenesis and adipogenic differentiation.

Materials and Methods

Patient samples

This study was approved by the Memorial Sloan Kettering Cancer Center (MSKCC) Institutional Review Board; all

[1]Department of Surgery, Memorial Sloan Kettering Cancer Center, New York, New York. [2]Microchemistry and Proteomics Core, Memorial Sloan Kettering Cancer Center, New York, New York. [3]Department of Epidemiology and Biostatistics, Memorial Sloan Kettering Cancer Center, New York, New York. [4]Bioinformatics Core Facility, Memorial Sloan Kettering Cancer Center, New York, New York. [5]Laboratory of RNA Molecular Biology, The Rockefeller University, New York, New York.

Note: Supplementary data for this article are available at Cancer Research Online (http://cancerres.aacrjournals.org/).

Corresponding Author: Samuel Singer, Memorial Sloan Kettering Cancer Center, 1275 York Avenue, Howard 1205, New York, NY 10065. Phone: 212-639-2940; Fax: 646-422-2300; E-mail: singers@mskcc.org

doi: 10.1158/0008-5472.CAN-16-2253

participants gave informed consent. Patient studies were conducted in accordance with the International Ethical Guidelines for Biomedical Research Involving Human Subjects and in accordance with MSKCC Institutional Review Board-approved protocol #02-060A. Patient characteristics are shown in Supplementary Table S1. Tumor and normal adipose tissue samples obtained during surgical resection were snap-frozen in liquid nitrogen and embedded in cryomolds.

Cell culture and reagents

Liposarcoma cell lines were established from patient tissue samples: DDLS8817, DD6960-1, and RDD8107 from DDLS samples; WD4847-2, RWD5700, and WD7785-1 from WDLS samples. The cell lines were validated by array comparative genomic hybridization confirming 12q amplification. Primary human adipose tissue-derived stromal/stem cells (ASC) were isolated from subcutaneous fat samples from consenting patients as described (14). Cell lines were maintained as described (10). The sources of antibodies and other reagents are listed in Supplementary Table S2.

Transfection and luciferase assays

MiRNAs and siRNAs were transfected with Oligofectamine (Invitrogen) and RNAiMAX (Invitrogen). Cells were harvested 72 hours after transfection for protein and mRNA analysis. Vectors for protein overexpression were transfected with Lipofectamine 3000 (Invitrogen) 1 day after miRNA transfection. Cells were collected for assays of protein, cell proliferation, and apoptosis on day 3 after miRNA transfection.

For luciferase reporter assays, 50 nmol/L miRNA and 200 ng of 3′UTR reporter plasmids were cotransfected with Lipofectamine 2000 (Invitrogen). At 48 hours posttransfection, cells were collected for luciferase assays according to Promega's instructions.

RNA isolation and analysis

Total RNA was isolated from cultured cells and analyzed as previously described (15). TaqMan gene expression assays (Life Technology) were used for relative gene expression (Supplementary Table S3). miRNA expression levels were detected by using SYBR Green miRNA-specific primers (Supplementary Table S3). Transcript levels were normalized to levels of GAPDH transcript (for mRNAs) or U6 snRNA (for miRNAs).

Immunoblotting

Cells were lysed in RIPA buffer (with 100× protease inhibitor cocktail and 25 μmol/L MG132) for 30 minutes on ice and sonicated to shear DNA. Protein concentration was determined by the Lowry method. Equal amounts of total protein were loaded and resolved by SDS-PAGE, then transferred to polyvinylidene difluoride membranes for immunoblotting. Secondary antibodies (horseradish peroxidase–conjugated) were detected using Western Lightning chemiluminescence reagent (PerkinElmer).

Cell viability, cell cycle, apoptosis analysis, and soft agar assays

Cells were treated with miRNAs, siRNAs, or FAK inhibitors. Cell viability was assessed using CellTiter-Glo luminescent cell viability assay (Promega). At 72 hours posttransfection, cell-cycle analysis was performed as previously reported (16). Apoptosis was quantified using a Muse Annexin V and Dead Cell Kit (EMD Millipore).

Soft agar assays were performed in 6-well tissue culture plates by placing miRNA- or siRNA-treated cells (2×10^4/well) in 2 mL of 0.3% soft agar above a 2-mL layer of 0.5% agar. The wells were covered with 1 mL fresh medium. Cell growth medium was exchanged every 2 days. After 2 weeks' incubation, cells were stained with 1 mg/mL MTT in medium for 1 hour. Colonies were detected and counted using GelCount technology (Oxford Optronix Inc.).

Adipogenic differentiation

Adipogenic differentiation was induced with initiating medium (regular growth medium plus 100 nmol/L insulin, 1 μmol/L dexamethasone, 250 μmol/L 3-isobutyl-1-methylxanthine, 33 μmol/L biotin, 17 μmol/L pantothenic acid, and 5 μmol/L of the PPARG agonist rosiglitazone). After 4 days, media were changed to maintenance medium (initiating medium without 3-isobutyl-1-methylxanthine or rosiglitazone). Cells were fed with maintenance medium every 4 days thereafter. After 12 days of adipogenic induction, cytoplasmic lipid droplets were stained with Oil Red O as described (17) and with DAPI. Stained cells were quantified by manual counting under a microscope. Three biological replicates were analyzed for each treatment group. At least 400 cells that were positive for lipid droplets were counted in each group.

ROS measurements and protein oxidation detection

ROS measurement was performed 48 hours after transfection by using H_2DCFDA (Molecular Probes, Invitrogen) according to the manufacturer's instructions. At 48 hours after transfection, the cells were treated with 10 μmol/L H_2DCFDA (Molecular Probes, Invitrogen) and incubated for 30 minutes at 37°C. Cells were washed, then plated at 10^4 cells/well in 96-well plates. The fluorescence intensity (excitation = 485 nm; emission = 530 nm) was measured by a SpectraMax L microplate reader (Molecular Devices).

For assessment of protein oxidation, lysates were prepared as described for immunoblotting. Total protein was incubated with 2,4-dinitrophenylhydrazine according to the instructions for the OxyBlot oxidized protein kit (Chemicon). β-Actin was used as a loading control.

Solexa sequencing

Small RNA cDNA libraries were prepared from 145 DDLS, 93 WDLS, and 12 normal fat tissue samples, as previously described (10). Data were normalized using the edgeR calcNormFactors function. The normalized counts were rescaled back to the geometric mean (mean of logs) of the raw data. The mean clone counts were also the geometric mean.

Microarray analysis

Illumina arrays were used to generate triplicate gene expression profiles in DD8817 and WD4847-2 cell lines 3 days after transfection with miR-193b or scramble miRNA. The expression profiles were processed using the LUMI package (Bioconductor) with the default options: background subtraction, normalization with the quantile method, and $\log_2$ transformation of expression values. Data were normalized using the variance-stabilization method (lumiExpresso). LIMMA (Bioconductor) was used to compute differential expression, and the false discovery rate (FDR) method was used for multiple testing corrections. The

microarray data are available from GEO (accession number GSE83690).

SILAC assay

DD8817 and WD4847-2 cells were grown in media supplemented with either unlabeled L-arginine and L-lysine at 50 mg/L (light medium) or equimolar amounts of the isotopic variants [U-$^{13}C^6$]-L-arginine (Arg6) and [U-$^{13}C^6$]-L–lysine HCl (Lys6; heavy medium; Cambridge Isotope Laboratories). After five cell doublings, cells were >99% labeled with the isotopes. Cells grown in the light medium were transfected with 50 nmol/L miR-193b mimic, while those grown in heavy medium were transfected with scramble miRNA control. Total protein from light and heavy labeled cells (10 mg each) was mixed. Cysteine residues were reduced and alkylated, then protein was digested with trypsin. Digested protein was centrifuged to pellet precipitated lipids and cleared supernatant desalted on a SepPak C18 cartridge 500 mg (Waters). Desalted peptides were separated through strong cation exchange chromatography and analyzed by the Q-Exactive mass spectrometer (Thermo Fisher Scientific). All MS/MS samples were analyzed by the Proteomics and Microchemistry Core Facility at MSKCC using MaxQuant (technical details are given in Supplementary Methods).

Methylation-specific PCR

Genomic DNA was extracted from L090310 and liposarcoma cell lines using the DNeasy Blood and Tissue Kit (Qiagen). DNA methylation status was established by methylation-specific PCR as described (18). Briefly, bisulfite conversion of DNA was performed by using the EpiTect Bisulfite Kit (Qiagen). As positive control, we used CpGenome Universal Methylated DNA (Chemicon/Millipore). PCR was performed in a thermal cycler using the EpiTect MSP Kit (Qiagen) with the following cycling conditions: 95°C for 10 minutes; then 35 cycles of 94°C for 15 seconds, 52°C for 30 seconds, 72°C for 30 seconds; then final extension of 10 minutes at 72°C.

Chromatin immunoprecipitation

To test DNMT1 binding of the miR-193b promoter, chromatin immunoprecipitation (ChIP) analysis was performed in WD4847-2 cells. Briefly, after cells were exposed to crosslinking with 1% formaldehyde for 10 minutes at room temperature, chromatin was purified and sonicated until the DNAs were around 500 bp long. ChIP was performed using the ChIP-IT High Sensitivity Kit (53040, Active Motif) with ChIP-grade DNMT1 antibody (39204) and native IgG, according to the manufacturer's instructions. DNA was analyzed via quantitative PCR. All ChIP experiments were completed with two biological replicates.

Xenograft studies

ICR SCID mice (Taconics) were implanted subcutaneously with serially transplanted DDLS8817 tumors, together with Matrigel. After palpable tumors developed (typically 100–150 mm^3), mice were ready for miRNA or drug treatment. For the miRNA study, 6.25 μg of synthetic miRNA-193b or control miRNA was complexed with 1.6 μL siPORT Amine transfection reagent (Ambion) in PBS and delivered intratumorally 8 times at 3-day intervals into 8 mice/group, as described (19). For the FAK inhibitor study, 5 mice/group received either vehicle (0.5% Tween-80 and 1% hydroxypropyl methylcellulose) or PF-562271 (50 mg/kg in vehicle) by oral gavage twice per day for 3 weeks. Tumors were measured twice per week using calipers. All animal care was in accordance with the Institutional Animal Care and Use Committee at MSKCC (protocol # 02-09-024).

Statistical analysis

Data for all experimental groups are presented as means ± SE. Statistical significance was assessed using the Student *t* test, and *P* values < 0.05 were taken as statistically significant.

Results

miR-193b is underexpressed in liposarcoma

We applied deep RNA sequencing to 93 WDLS, 145 DDLS, and 12 normal fat samples. The 50 miRNAs most differentially expressed between DDLS and normal fat (Supplementary Table S4) were subjected to unsupervised hierarchical clustering (Fig. 1A). Three miR-193 family members were underexpressed in DDLS compared with normal fat. miR193b was underexpressed

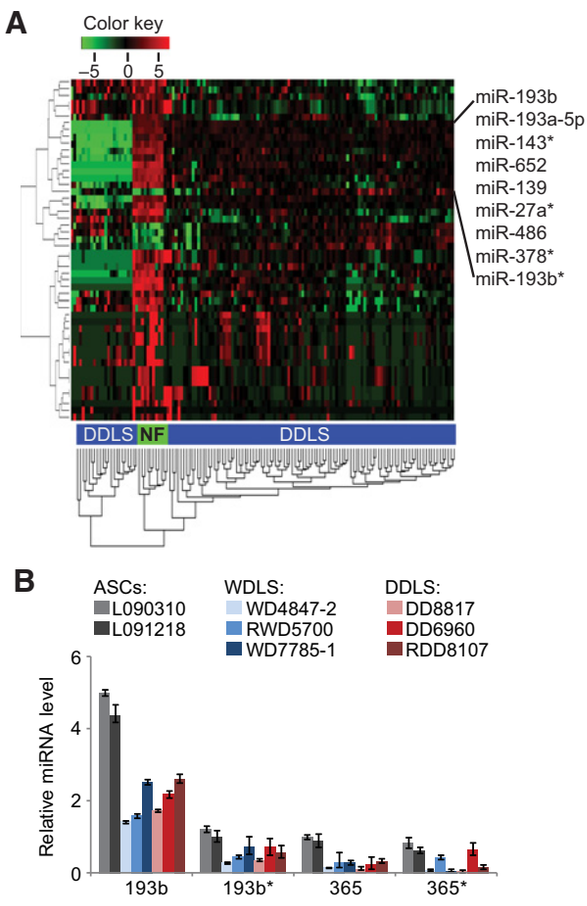

Figure 1.

The miR-193b/365 cluster is underexpressed in liposarcoma. **A,** Heat map of the 50 most differentially expressed miRNA profiles in DDLS tissue compared with normal fat (NF). Columns, profiled DDLS and NF tissue samples; rows, miRNAs ordered by unsupervised clustering. The details of heatmap constructions are in Supplementary Methods. **B,** miRNA expression in cell lines. The values (normalized to miR-365 in L090310 cells) represent the mean ± SE of three independent experiments.

by 9-fold (FDR = 0.006; Supplementary Fig. S1A). Among patients with primary WDLS or DDLS, miR-193b expression was associated with distant recurrence-free survival (HR = 0.58, P = 0.015; Fig. Supplementary S1B).

miR-193b derives from the same primary transcript as another miRNA, miR-365. Both these miRNAs were downregulated approximately 2-to 3-fold in multiple liposarcoma cell lines derived from liposarcoma tissues compared with normal ASCs (Fig. 1B).

miR-193b is a tumor suppressor in liposarcoma cells, while it promotes adipogenic differentiation in ASCs

We investigated miRNA function by introducing miRNAs into liposarcoma cells and ASCs. miR-193b mimic significantly inhibited proliferation of liposarcoma cells, but not ASCs (Fig. 2A; Supplementary Fig. S2). miR-193b mimic repressed multiple cell-cycle regulators (Fig. 2B) and induced increases in the G_0–G_1 population (Fig. 2C), implying G_0–G_1 arrest. miR-193b also induced significant apoptosis in liposarcoma cells (Fig. 2D and E). Furthermore, miR-193b strongly inhibited anchorage-independent growth of liposarcoma cells (Fig. 2F). miR-365 mimic had weaker effects.

Next, we assessed whether the miR-193b/365 cluster regulates adipogenic differentiation. During induction of adipogenesis in ASCs (Fig. 2G), miR-193b and miR-365 levels increased about 16 fold (Fig. 2H). miR-193b mimic markedly upregulated adipogenic markers (Fig. 2I). Consistent with this, miR-193b mimic promoted the formation of lipid droplets, while miR-193b inhibitor (anti-miRNA) completely blocked this effect (Fig. 2J). miR-365 showed no effects on differentiation. These results indicate that miR-193b functions as a tumor suppressor in liposarcoma and an activator of adipogenesis in ASCs.

Identification of miR-193b targets

To identify miR-193b targets, we carried out mRNA microarray and SILAC analysis in miR-193b–treated cells. Similar to a prior study (15), the frequency of downregulated genes or proteins (fold change ≤ -1.5, FDR < 0.05) was no more than 10% (Supplementary Table S5A and S5B). In contrast to non-predicted genes, the majority of predicted miR-193b target genes exhibited reductions in both protein and mRNA levels (Fig. 3A; Supplementary Fig. S3A and S3B). Eight known targets of miR-193b (20, 21) showed downregulation by miR-193b in either our microarray or SILAC analysis (Table S5C).

We developed a strategy to identify miR-193b targets and the processes affected by them in liposarcoma (Fig. 3B). Eight target prediction programs (DIANA-mT, miRDB, miRanda, miRWalk, RNAhybrid, PICTAR5, RNA22, Targetscan; refs. 20–28) were applied to reduce bias. There were 2,056 genes predicted to be miR-193b targets by at least 3 of the 8 prediction programs. Among these 2,056 were 50 genes were downregulated in our SILAC analysis in DD8817 or WD4847-2 cells (fold change ≤ -1.5, FDR < 0.05; Supplementary Table S6). These 50 genes, subjected to gene ontology enrichment analysis, were significantly associated with multiple biological processes and molecular functions ($P \leq 0.05$;Supplementary Fig. S3C, S3D, and Supplementary Table S7). The KEGG pathway annotations of these target genes revealed enrichment of several pathways, including focal adhesion, regulation of actin cytoskeleton, and pyrimidine metabolism ($P < 0.05$, Fig. 3C). Four of these pathways involved the putative miR-193b targets CRKL and FAK (focal adhesion kinase; HUGO name PTK2), so we investigated these genes further.

CRKL is the direct target of miR-193b

CRKL plays important roles in signal transduction in cancer (29). To test whether it is a direct target of miR-193b, we constructed CRKL 3′UTR reporters. miR-193b mimic inhibited the luciferase activity of wild-type reporter, but not of reporter bearing seed site mutations (Fig. 3D). Furthermore, miR-193b mimic repressed mRNA and protein levels of CRKL, while addition of anti-miRNA completely blocked the effect on the protein level (Fig. 3E). These results demonstrated that miR-193b directly targets CRKL. Overexpression of CRKL partially blocked the miR-193b–induced cell growth inhibition and apoptosis (Fig. S4A–C), providing evidence that derepression of CRKL is responsible in part for the effects of low miR-193b expression in liposarcoma cells.

siRNA knockdown of CRKL significantly repressed cell proliferation in liposarcoma cells (Fig. 3F). Similar to miR-193b transfection, CRKL knockdown induced G_0–G_1 phase arrest, inhibited multiple cell-cycle regulators (Fig. 3G; Supplementary Fig. S4D), and induced substantial apoptosis (Fig. 3H). Furthermore, CRKL knockdown reduced colony formation of DD8817 cells by 90% (Fig. 3I). CRKL has been reported to mediate signaling of FAK through SRC family kinases (30). Consistent with this, CRKL knockdown repressed the phosphorylation of FAK and SRC (Fig. 3J). Taken together, these results indicate that inhibition of CRKL may suppress liposarcomagenesis.

miR-193b regulates tumorigenesis and adipogenic differentiation through directly targeting FAK

In a test for direct targeting of FAK, miR-193b repressed more than 80% of the activity of a wild-type FAK 3′UTR reporter, but did not affect reporter bearing seed-site mutations (Fig. 4A). miR-193b mimic inhibited FAK expression, while miR-193b inhibitor blocked the effect on protein (Fig. 4B). Thus, miR-193b directly regulates FAK. Knockdown of FAK induced significant cell growth inhibition, G_0–G_1 phase arrest (40%–80%), and apoptosis (Fig. 4C–E). Restoring FAK expression through exogenous overexpression significantly reduced miR-193b–induced growth inhibition and apoptosis (Fig. S5A–C). These observations demonstrate the oncogenic function of FAK in liposarcoma cells.

To define the molecular mechanisms of FAK function in liposarcoma, we assessed the regulation of effectors of FAK signaling. miR193b mimic strongly repressed phosphorylation of both SRC and BCAR1, which are phosphorylated by FAK (31), while miR-193b inhibitor blocked this inhibition (Fig. 4F). Similar regulation was observed with FAK knockdown (Fig. 4G). These results suggest that miR-193b regulates oncogenic FAK–SRC–BCAR1 signaling in liposarcoma through directly targeting FAK.

Next, we tested two FAK inhibitors, PF-573228 (PF-228) and PF-562271 (PF-271). Both inhibitors strongly repressed FAK activation as measured by phosphorylation of FAK, SRC, and BCAR1 (Fig. 4H). These compounds inhibited cell growth (Fig. 4I) and induced apoptosis in liposarcoma cells (Fig. 4J). Furthermore, both FAK siRNA and FAK inhibitor (PF-271) not only resulted in upregulation of adipogenic makers (Fig. 4K), but also induced 2.5- to 3.5-fold increases in lipid droplet formation (Fig. 4L). These results show that FAK inhibition suppresses tumor activity and promotes adipogenic differentiation in normal ASCs.

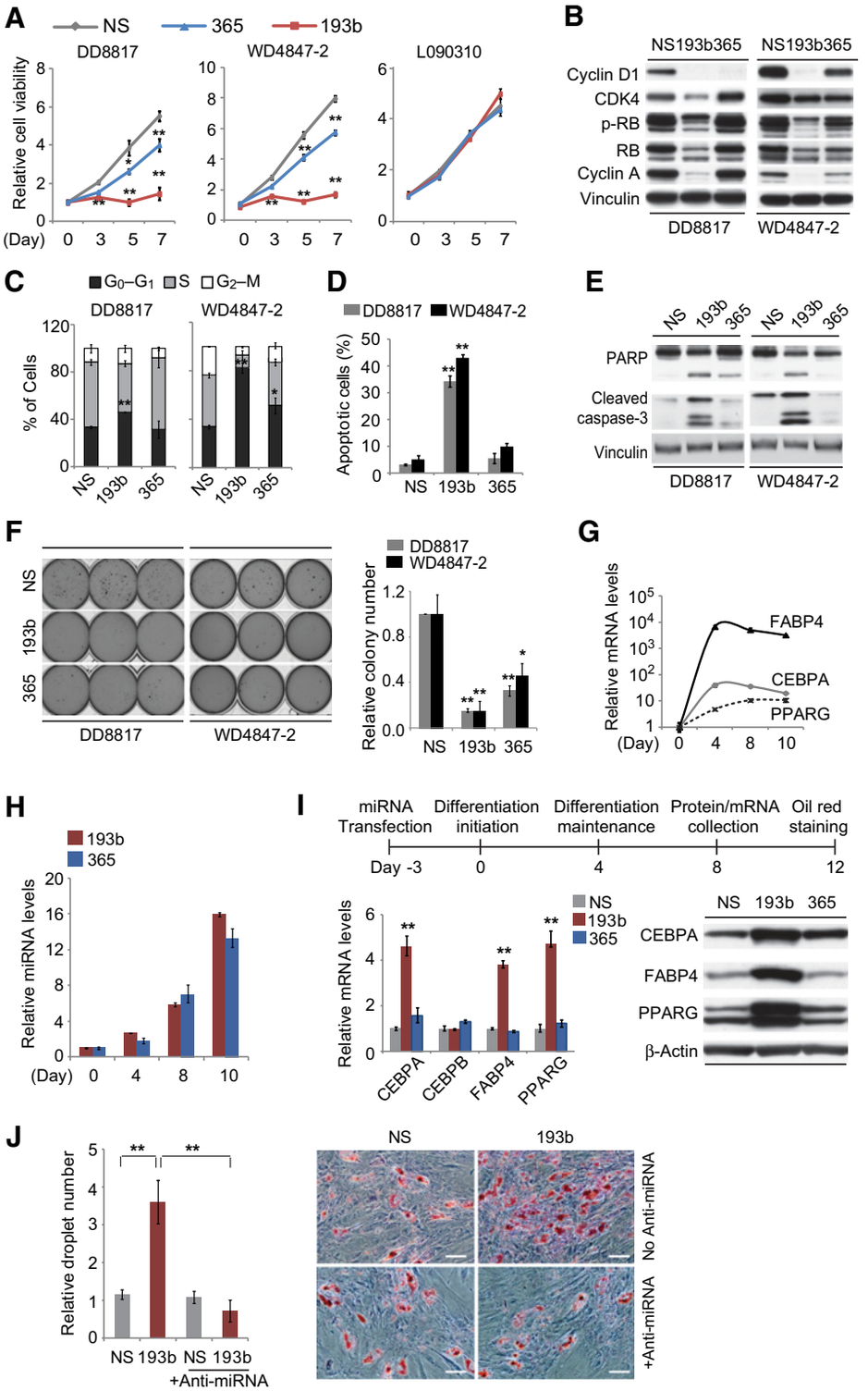

Figure 2.
miR-193b functions as a tumor suppressor and promotes adipogenic differentiation. **A,** Cell proliferation after transfection of miRNAs or nonspecific (NS) control. **B,** Levels of cell-cycle regulatory proteins by immunoblots. **C,** Flow cytometry analysis. **D,** Apoptosis of miR-193b–treated liposarcoma cells detected by Annexin V assays. **E**, Apoptotic markers detected by immunoblots. **F**, Soft-agar assays of miR-treated cells. The colony numbers were normalized to those in the control cells. **G** and **H,** levels of differentiation marker mRNAs and miR-193b/365 during adipogenic differentiation. Values were normalized to day 0. **I**, Effects of miR-193b on adipogenic differentiation markers. The diagram summarizes the adipogenic differentiation procedure, which began 3 days after transfection. Protein and mRNA were analyzed on day 8 of differentiation. Gene expression values were normalized to the NS group. **J**, Accumulation of lipid droplets during adipogenic differentiation in ASCs. Lipid droplets were detected by Oil Red O staining. The droplets numbers, normalized to the nonspecific controls, represent the mean ± SE of three independent experiments. *, $P < 0.05$; **, $P < 0.01$ vs. control groups. Scale bar, 25 μm.

miR-193b induces oxidative stress through targeting methionine sulfoxide reductase A

In liposarcoma cells, we found miR-193b increased levels of ROS by 2- to 4-fold, while the antioxidant *N*-acetylcysteine prevented most of this miR-193b–induced ROS increase (Fig. 5A) and apoptosis (Fig. 5B). Excessive ROS may induce mitochondrial damage, reflected by a loss of mitochondrial membrane potential ($\Delta\psi$m). Compared with control miRNA, transfected miR-193b induced mitochondrial membrane depolarization in about 30% of cells, indicating a significant reduction in mitochondrial

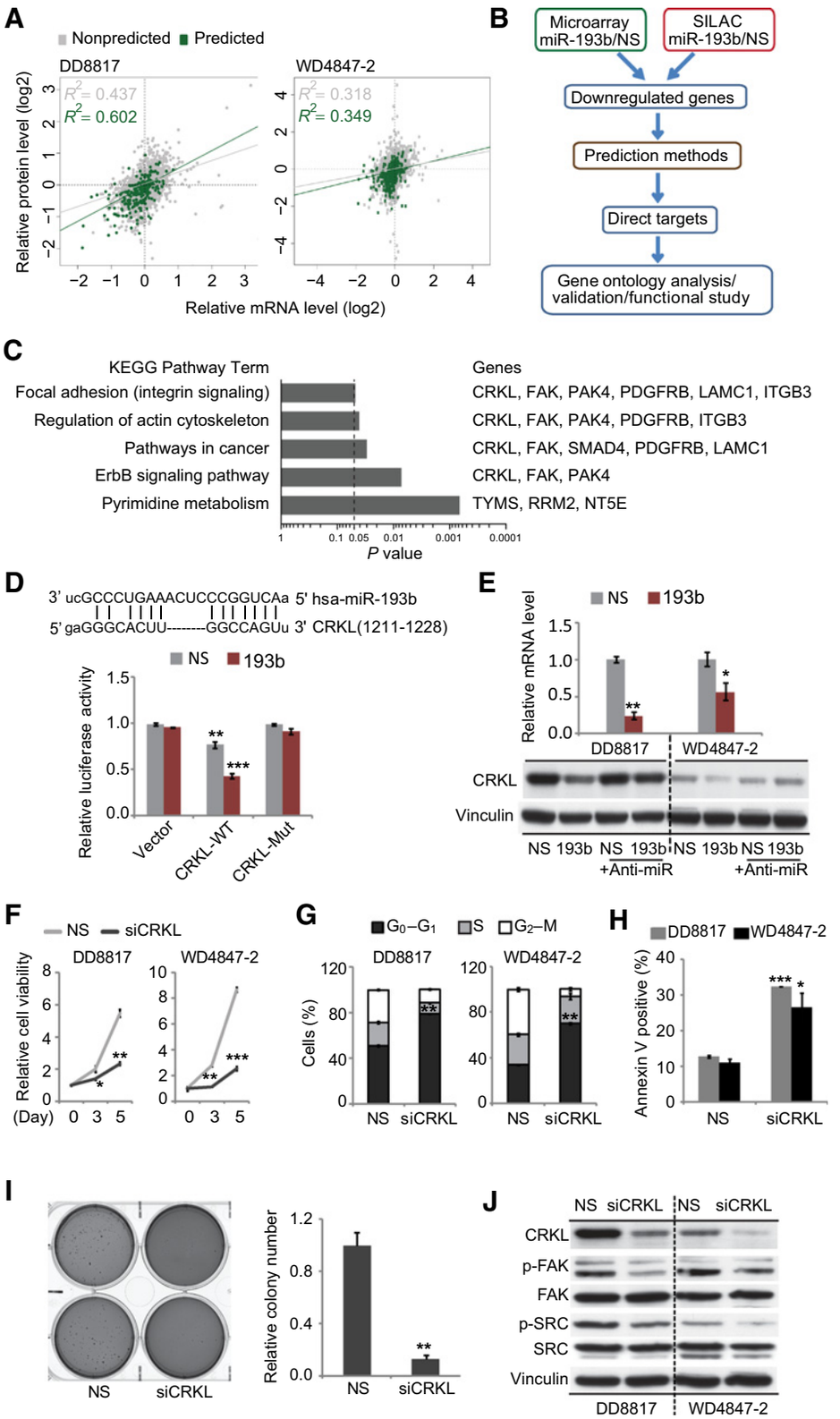

Figure 3.

Transcriptomic and proteomic changes induced by miR-193b. **A,** mRNA versus protein changes induced by miR-193b mimic. Green dots, predicted miR-193b target genes (via TargetScan); gray dots: non-target genes. The linear regression and Pearson correlation coefficient are shown for each set. **B,** Strategy to identify miR-193b targets and the processes they affect in liposarcoma. **C,** *P* values of pathways identified in KEGG pathway analysis. To the right are the relevant genes from the top 50 miR-193b targets. **D,** Effect of transfected miR-193b on the activity of wild-type CRKL 3′UTR reporter (CRKL-WT) and reporter in which miR-193b seed sites were mutated (CRKL-Mut). **E,** Effect of miR-193b (with or without anti-miRNA) on mRNA and protein levels of CRKL. **F–J,** Consequences of siRNA knockdown of CRKL in liposarcoma cells. **F,** Cell proliferation relative to day 0. **G,** Cell-cycle assays performed 48 hours after transfection of siCRKL. **H**, Apoptosis quantified by Annexin V assays 72 hours after siCRKL transfection. **I,** Anchorage-independent cell growth assessed by soft agar assay. Colony numbers were normalized to the control siRNA group. **J,** Activated and total FAK and SRC assessed by immunoblots after siRNA transfection. The values represent the mean ± SE of three independent experiments. *, $P < 0.05$; **, $P < 0.01$; ***, $P < 0.001$ versus control groups treated with vector (**D**) or with nonspecific (NS) miRNA or siRNA.

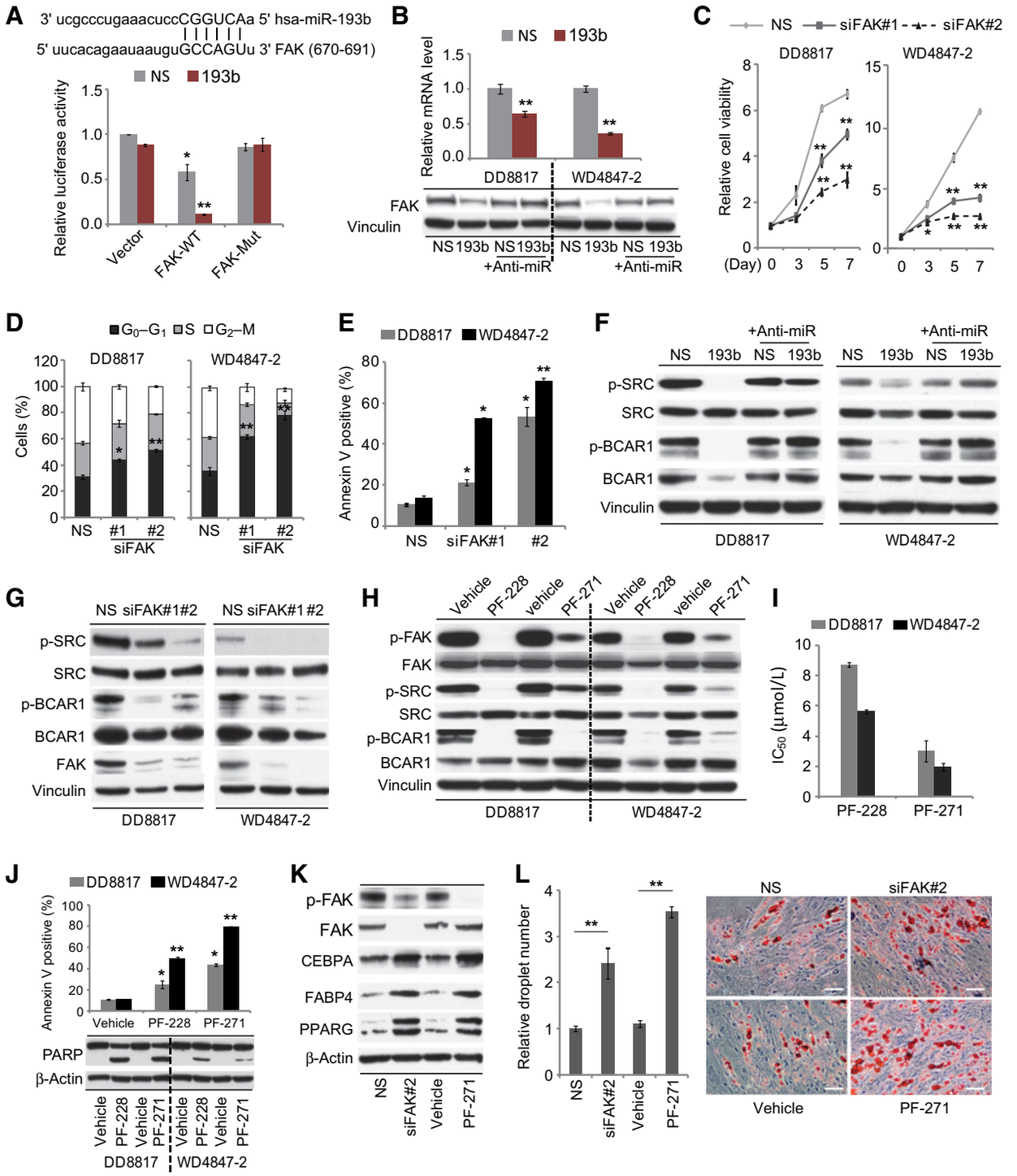

Figure 4.

Inhibition of FAK represses tumor cell growth and blocks adipogenic differentiation. **A,** Effects of miR-193b on wild-type (FAK-WT) and mutant (FAK-Mut) FAK 3′UTR reporters. **B,** FAK mRNA and protein levels in miRNA-treated liposarcoma cells. **C–E,** Effects of siRNA knockdown on FAK. **C,** Cell proliferation relative to day 0. **D,** Cell-cycle assays 48 hours after transfection of siFAK. **E,** Apoptosis quantified by Annexin V assays 72 hours after siFAK transfection. **F–H,** Effects of FAK inhibition in liposarcoma cells on the activation of FAK/SRC signaling, assessed by phosphorylation of SRC and BCAR1. **F,** miR-193b mimic (with or without anti-miR). **G,** siFAK. **H,** FAK inhibitors (10 μmol/L PF-228 or 5 μmol/L PF271). **I,** IC_{50} of PF-228 and PF-271 with respect to proliferation of liposarcoma cells. **J,** Apoptosis induced by FAK inhibitors. **K** and **L,** Effects of FAK inhibitors on adipogenesis of ASCs. Adipogenic differentiation markers were detected on day 12 of differentiation (**K**). Oil Red O staining was used to detect lipid droplets (**L**). All the values represent the mean ± SE of three independent experiments. *, $P < 0.05$; **, $P < 0.01$ versus control groups treated with vector (**A**), nonspecific (NS) miRNA or siRNA, or vehicle. Scale bar, 25 μm.

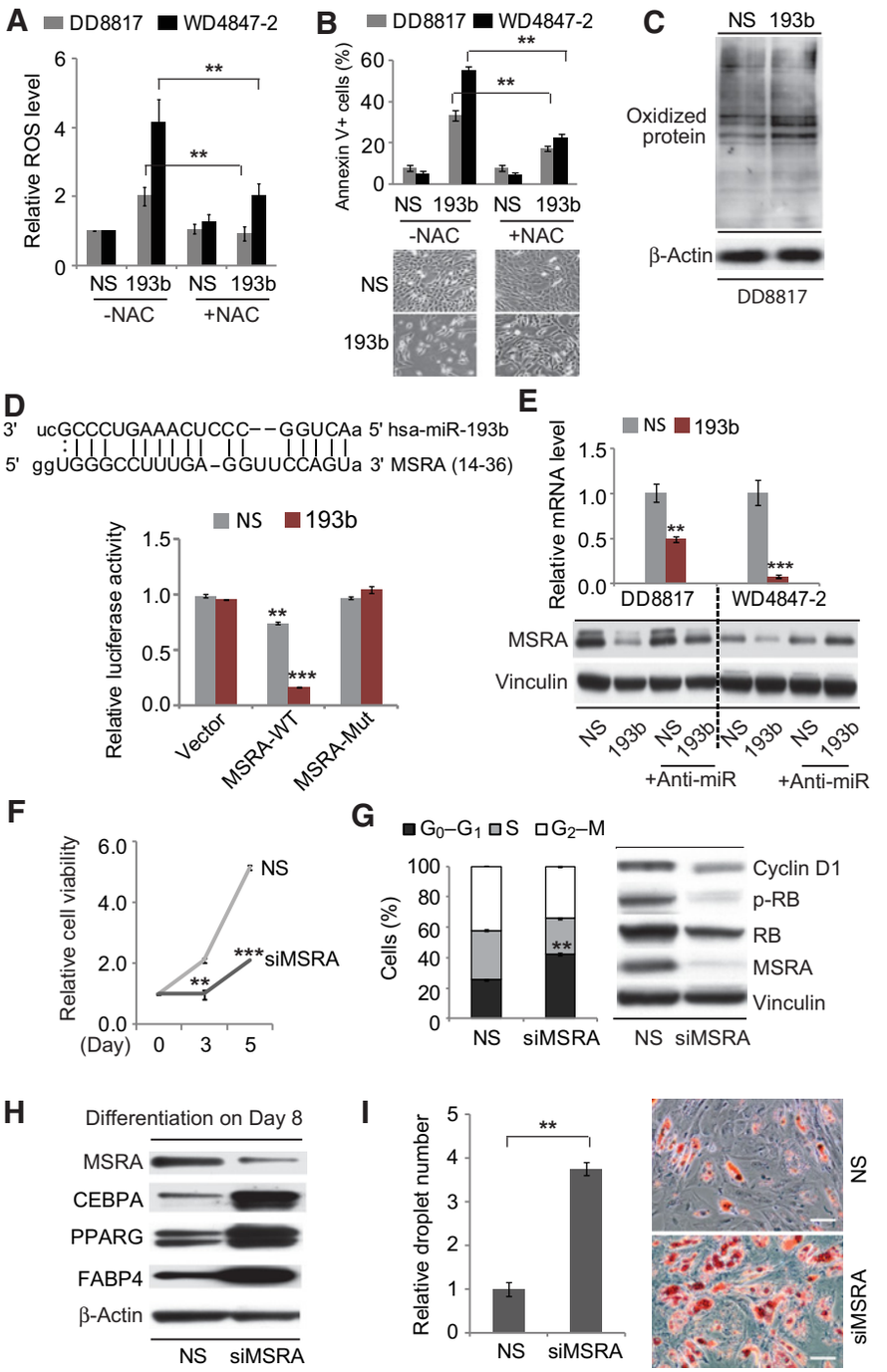

Figure 5.

miR-193b induces oxidative stress by targeting MSRA. **A,** ROS levels after treatment of cells with miRNA with or without *N*-acetylcysteine. Values were normalized to the nonspecific (NS) group. **B,** Apoptosis 72 hours after cells were treated with miRNA with or without *N*-acetylcysteine (5 mmol/L). Bottom, WD4847-2 cells visualized by phase-contrast microscopy; results with DDLS8817 were similar. **C,** General protein oxidation detected by OxyBlot. **D,** Effects of miR-193b on activity of wild-type MSRA 3′UTR reporter (MSRA-WT) and mutant reporter (MSRA-Mut). **E,** MSRA mRNA and protein levels detected in miRNA-treated cells. **F–I,** Consequences of knockdown of MSRA in liposarcoma cells. **F,** Cell proliferation relative to day 0. **G,** Cell-cycle assays and immunoblot of cell-cycle regulators 48 hours after transfection. **H** and **I,** Adipogenic differentiation after MSRA knockdown in ASCs. Adipogenic differentiation markers were detected by immunoblot on day 12 of differentiation (**H**). Oil Red O staining was used to detect lipid droplets; numbers were normalized to the nonspecific group (**I**). All the values represent the mean ± SE of three independent experiments. **, $P < 0.01$; ***, $P < 0.001$ versus control groups treated with nonspecific miRNA or siRNA. Scale bar, 25 μm.

membrane potential (Supplementary Fig. S6A and S6B). Addition of *N*-acetylcysteine reduced these effects. miR-193b mimic increased the level of protein oxidation in liposarcoma cells (Fig. 5C). These results demonstrate that miR-193b–induced ROS production induces mitochondrial damage and, consequently, apoptosis.

We inspected our microarray and SILAC data for genes involved in ROS signaling. The best candidate was methionine sulfoxide reductase A (MSRA), an antioxidant enzyme (32). 3′UTR reporter assays showed that miR-193b directly regulated MSRA through seed sites on the 3′UTR (Fig. 5D). miR-193b strongly reduced expression of MSRA at both protein and mRNA levels, and the repression of MSRA protein was reversed by addition of anti-miR-193b (Fig. 5E). Overexpression of MSRA significantly attenuated the miR-193b–induced increase in ROS production (Supplementary Fig. S7A and S7B). These results demonstrate that in liposarcoma cells miR-193b directly targets MSRA to regulate ROS signaling.

Knockdown of MSRA induced increases in ROS level (by 2-fold) and protein oxidation (Supplementary Fig. S7C and S7D).

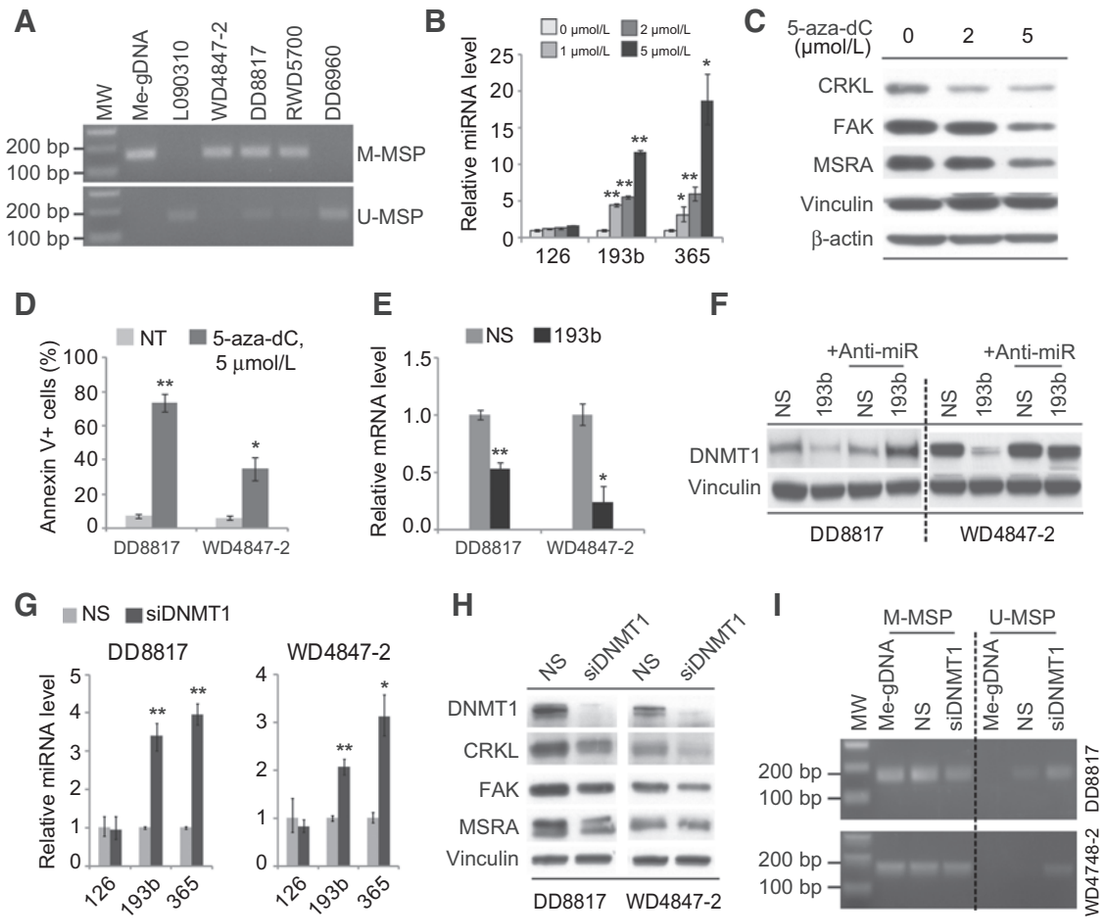

Figure 6.

Regulation of miR-193b by DNA methylation and regulation of DNMT1 by miR-193b. **A,** Extent of methylation of the miR-193b promoter in cells assessed by methylation-specific PCR. M-MSP, methylation-specific primers; U-MSP, primers specific to unmethylated DNA; Me-gDNA, enzymatically methylated genomic DNA, used as positive control for methylation. **B–D,** Effects of 5-aza-dC treatment for 48 hours on expression of miRNAs (**B**), expression of targets (**C**), and apoptosis (**D**). **E** and **F,** Expression of DNMT1 mRNA (**E**) and protein (**F**) at 72 hours after transfection of miRNA. **G** and **H,** Effects of siRNA knockdown of DNMT1 on expression of miRNAs (**G**) and miR-193b target proteins (**H**). **I,** Methylation of the miR-193b promoter as detected by methylation-specific PCR at 72 hours after knockdown of DNMT1 in liposarcoma cells. NS, nonspecific.

Furthermore, in WD4847-2 cells siMSRA significantly repressed cell growth (Fig. 5F) and induced G_0–G_1 phase arrest (Fig. 5G). In DD8817, in contrast, siMSRA induced only modest cell growth inhibition and G_0–G_1 cell accumulation (Supplementary Fig. S7E–S7G), suggesting that MSRA function may depend on specific molecular alterations or the cell differentiation state.

Elevated ROS levels are reported to be essential for adipogenic differentiation (33). MRSA knockdown strongly induced differentiation markers and formation of lipid droplets in ASCs (Fig. 5H and I). Furthermore, MSRA was downregulated during adipogenic differentiation in ASCs (Supplementary Fig. S7H). Taken together, these results imply that miR-193b, through targeting MSRA, induces ROS accumulation, affecting apoptosis in liposarcoma cells and adipogenic differentiation in ASCs.

The DNA methyltransferase DNMT1 regulates miR-193b target networks

We previously observed hypermethylation of the miR-193b promoter in a small set of liposarcomas (34). In this study, we applied unbiased genome-wide methylation sequencing in 13 DDLS, 21 WDLS, and 8 normal fat tissue samples. The miR-193b promoter was methylated in both DDLS and WDLS tissues, but mostly unmethylated in normal fat (Fig. S8A). The liposarcoma tissues also had decreased miR-193b levels (Fig. S8B), suggesting that DNA methylation may contribute to the silencing of miR-193b in liposarcoma.

Methylation-specific PCR was used to analyze methylation of miR-193b promoter. Primer specificity was confirmed by using completely methylated human genomic DNA (Supplementary Figs. S8C and S6A). In three of four liposarcoma cell lines, the promoter was amplified by methylation-specific primers; two of these were also weakly amplified by primers specific for unmethylated DNA (Fig. 6A). Conversely, the promoter in normal ASCs was amplified only by the unmethylation-specific primers. To test whether promoter hypermethylation contributes to the downregulation of miR-193b in liposarcoma cells, we used a DNA methyltransferase inhibitor, 5-aza-2′-deoxycytidine (5-aza-dC; decitabine). As reported previously (16), upregulation of CEBPA

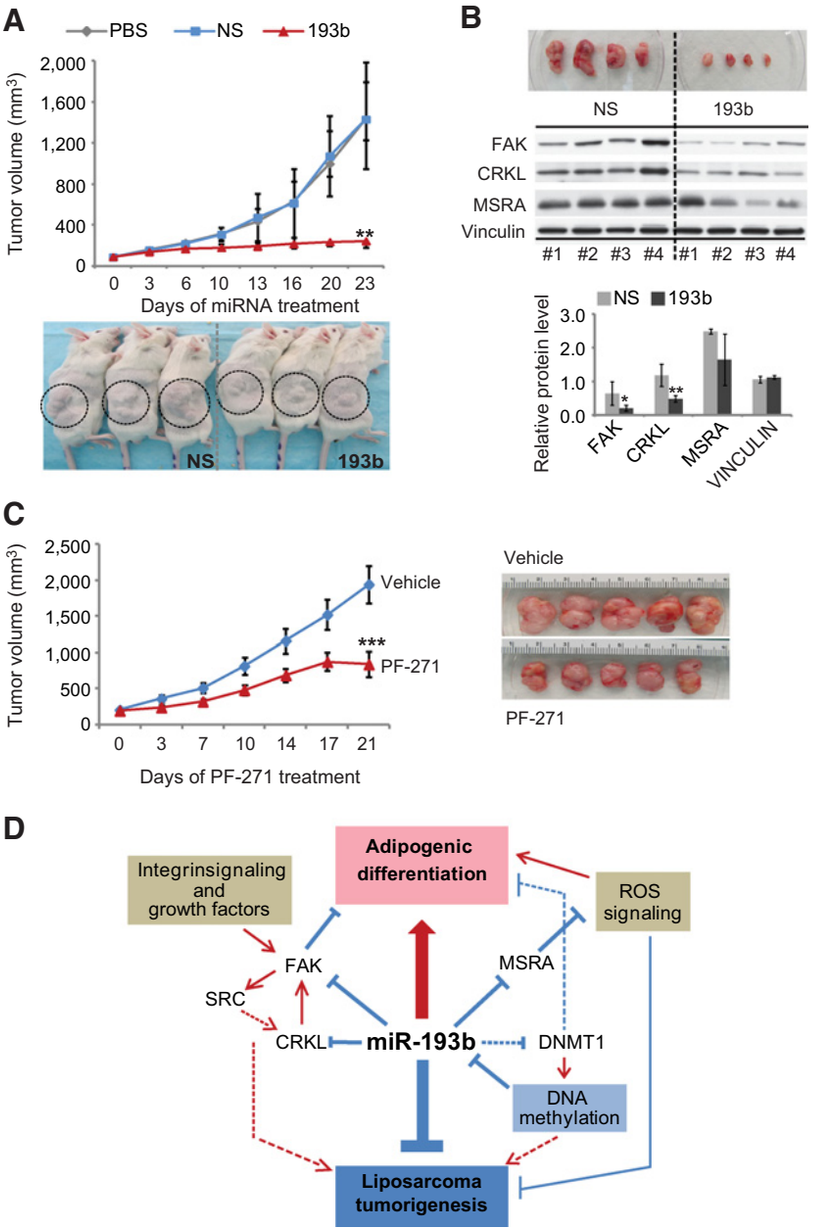

Figure 7.

Antitumor effects of miR-193b and FAK inhibitor (PF-271) *in vivo*. **A,** Effect of miR-193b on tumor growth. Tumor volumes were measured following intratumoral injection of PBS, nonspecific (NS)-miRNA, or miR-193b into established DD8817 xenograft tumors ($n = 5$ for each group). **B,** Inhibition of miR-193b targets *in vivo*. Four representative tumors for each group were subjected to immunoblotting; band density was quantified using ImageJ, and protein levels were normalized to vinculin. **C,** Effect of PF-271 on liposarcoma growth. Tumor volumes were measured following intratumoral injection of vehicle or PF-271 (50 mg/kg) into established DD8817 xenograft tumors ($n = 5$ for each group). **D,** Schematic representation shows the functions of miR-193b in liposarcoma and normal mesenchymal stromal cells. Solid lines indicate direct regulation, and dashed lines indicate indirect regulation, as demonstrated in this study or prior studies. Values are means ± SE. *, $P < 0.05$; **, $P < 0.01$; ***, $P < 0.001$ versus treatment with nonspecific miRNA or vehicle.

was induced by 5-aza-dC (Supplementary Fig. S8D). 5-Aza-dC treatment also caused dose-dependent increases of 3- to 15-fold in the miR-193b and miR-365 levels (Fig. 6B). The miR-193b targets (CRKL, FAK, and MSRA) were downregulated with 5-aza-dC treatment (Fig. 6C). Furthermore, Annexin V assays showed that 5-aza-dC induced apoptosis in DD8817 (74%) and WD4847-2 (35%; Fig. 6D). Thus, pharmacologic inhibition of methylation in liposarcoma cells reverses several of the effects of miR-193b underexpression.

In data from our earlier microarray analysis of mRNA in WDLS/DDLS tissue samples versus normal fat (35), DNMT1 expression was elevated on average 3-fold in DDLS and 2-fold in WDLS. In addition, DNMT1 was highly expressed in most liposarcoma cell lines compared with ASCs (Supplementary Fig. S8E). Intriguingly, DNMT1 was strongly downregulated by miR-193b in both microarray and SILAC analyses. Transfected miR-193b strongly repressed DNMT1 expression (Fig. 6E and F). However, multiple miRNA-target prediction tools found no miR-193b seed sites in the DNMT1 3′UTR region.

Similar to 5-aza-dC treatment, DNMT1 knockdown specifically increased miR-193b/365 expression by 2- to 4-fold (Fig. 6G). Correspondingly, DNMT1 knockdown resulted in downregulation of miR-193b targets (Fig. 6H). ChIP analysis demonstrated that DNMT1 directly bound to the miR-193b promoter, and 5-aza-cD treatment markedly reduced this binding (Supplementary Fig. S8F). DNMT1 knockdown resulted in partial demethylation of the miR-193b promoter, as evidenced by amplification by unmethylation-specific primers (Fig. 6I). However, the demethylation was not complete, suggesting that other genes may also regulate miR-193b promoter methylation. During

adipogenic differentiation of ASCs, DNMT1 was strongly downregulated (Fig. S8G) while miR-193b was upregulated (Fig. 2H), which supports the idea that DNMT1 regulates methylation of the miR-193b promoter during differentiation.

miR-193b and FAK inhibitor suppress liposarcoma growth *in vivo*

To assess the antitumor activity of miR-193b *in vivo*, mice bearing subcutaneous DD8817 tumor xenografts were treated by intratumoral miR-193b injections, which resulted in a 14-fold increase in the miR-193b level (Supplementary Fig. S9A). After 3 weeks of treatment, miR-193b–injected mice had significantly lower tumor volume (242 mm^3) than those receiving the control miRNA injections (1,431 mm^3), without significant difference in body weight of the mice (Fig. 7A and Supplementary S9B). The miR-193b–treated xenografts showed reduced Ki-67 staining (Supplementary Fig. S9C). Three miR-193b targets (CRKL, FAK, and MSRA) had reduced protein levels in the miR-193b–injected tumors (Fig. 7B). These results demonstrate that miR-193b has antitumor effects *in vivo* in a human liposarcoma xenograft model.

We also evaluated the FAK inhibitor PF-271 *in vivo*. After 3 weeks of treatment of DD8817-xenografted mice, tumor growth was inhibited more than 50% in PF-271-treated mice compared with vehicle-treated mice (Fig. 7C), while body weight was not affected (Supplementary Fig. S9D). Phosphorylation of FAK, SRC, and BCAR1 was markedly inhibited, demonstrating that PF-271 inhibited FAK and its downstream effectors (Supplementary Fig. S9E).

Discussion

In this study, we demonstrated the significance of miR-193b in liposarcoma. miR-193b, by directly targeting FAK, CRKL, and MSRA, regulates focal adhesion signaling and ROS signaling, which play pivotal roles in liposarcomagenesis and adipogenic differentiation (Fig. 7D). In addition, we showed that DNMT1 upregulation in WDLS and DDLS promotes miR-193b promoter methylation, leading to miR-193b underexpression in liposarcoma (Fig. 7D). To our knowledge, this is the first demonstration of the tumor suppressive activity of miR-193b in liposarcoma, and of the oncogenic roles of FAK–SRC–CRKL signaling and MSRA-regulated ROS signaling in liposarcoma.

A strength of this study is that the miRNA profiles were derived from 145 patient samples, which to our knowledge is a much larger number than in prior studies of miRNAs in liposarcoma. Our study confirmed prior reports (9, 11, 12) of dysregulation in liposarcoma for miR-143, miR-145, miR-451, and miR-486 (Supplementry Table S2 and data not shown).

Of the 50 miRNAs most differentially expressed in DDLS tissues in our analysis, 45 were underexpressed. This general downregulation of miRNAs in liposarcoma could be explained in part by the downregulation of Dicer that has been observed in liposarcoma (8).

Two of the direct miR-193b targets (FAK and CRKL) are known to be upregulated in multiple tumor types. FAK regulates cell motility, the cell cycle, survival, and differentiation in many cell types (31). CRKL, along with other CRK family members, is closely associated with FAK–SFK signaling (30). Thus, in the FAK–SFK signaling network, miR-193b directly inhibits both upstream FAK and downstream CRKL signal transduction. CRKL is upregulated in numerous cancer types (29). However, there is limited knowledge of miRNA regulation of CRKL (29), and only four miRNAs (miR-126 and miR-200b/200c/429) were previously identified as direct regulators of CRKL (36, 37). In liposarcoma cells, inhibition of CRKL and FAK significantly represses activation of FAK–SRC signaling, resulting in cell-cycle arrest and apoptosis. Similar to miR-193b, the FAK inhibitor (PF-271) strongly inhibits DDLS tumor growth in mice. This demonstrates that FAK inhibitors have therapeutic potential in DDLS with reduced miR-193b expression.

Besides FAK–SRC–CRKL signaling, we also defined the function of ROS signaling in liposarcoma cells, which miR-193b regulates by targeting MSRA. Cross-talk between ROS signaling and FAK–SRC signaling may be a means by which miR-193b regulates tumorigenesis and differentiation. Although ROS, as external or internal cell stimuli, can activate FAK, prolonged oxidative stress induces FAK cleavage and apoptosis (38, 39). Normal ASCs have lower levels of FAK and CRKL than liposarcoma cells, and they may not be as dependent on FAK–SRC–CRKL signaling for survival, because inhibition of FAK or CRKL does not induce significant cell death in ASCs (data not shown). The fact that overexpression of FAK, CRKL, or MRSA only partially rescued cells from the effects of exogenous miR-193b implies that all three of these proteins contribute to the miR-193b–related phenotypes in liposarcoma. Both repression of FAK and increased production of ROS have been reported to favor adipogenic differentiation of mesenchymal stromal cells (31, 40). Therefore, miR-193b–induced inhibition of FAK and elevation of ROS determine the different fates of tumor cells and ASCs, inducing cell death in tumor and adipogenic differentiation in ASCs.

DNA methylation silences numerous cancer-related genes, including miRNAs. Although methylation of the miR-193b promoter has been reported in several tumors (34, 41, 42), the mechanisms were not determined. We found that DNMT1 is upregulated in WDLS and DDLS cells and binds to the miR193b promoter, resulting in promoter methylation and decreased miR-193b expression. The decreased miR-193b expression in liposarcoma likely results from the action of multiple regulators. For example, DNMT1 may not be the only DMNT contributing to methylation of the miR-193b promoter, as knockdown of DNMT1 did not fully abolish its methylation. Besides DNMTs, histone modification or other factors could also regulate miR-193b expression. Interestingly, inhibition of DNMT1 was reported to promote adipogenic differentiation (43), suggesting that inhibition of DNMT1-induced miR-193b promoter methylation increased miR-193b expression, which in turn enhanced adipogenic differentiation. The strong inhibition of DNMT1 by miR-193b could result from direct binding to seed sites outside the 3′UTR of DNMT1 or indirect regulation via targeting regulators of DNMT1 expression. All these possibilities will be explored more in our future studies.

In conclusion, this study elucidates several interconnected mechanisms of molecular dysregulation in liposarcomas, with miR-193b modulating liposarcomagenesis and adipogenic differentiation at multiple levels. Our findings suggest possible therapeutic benefit of tumor-targeted miR-193b in liposarcomas with low miR-193b expression. Furthermore, small-molecule inhibitors of FAK and DNA methylation may be useful therapeutic strategies for combination therapy of liposarcoma.

Disclosure of Potential Conflicts of Interest

No potential conflicts of interest were disclosed.

Authors' Contributions

Conception and design: Y.Z. Mazzu, S. Singer
Development of methodology: Y.Z. Mazzu, Y. Hu, R.K. Soni, T. Tuschl, S. Singer
Acquisition of data (provided animals, acquired and managed patients, provided facilities, etc.): Y.Z. Mazzu, Y. Hu, K.M. Mojica, Z.M. Waxman, A. Mihailovic, R.C. Hendrickson, S. Singer
Analysis and interpretation of data (e.g., statistical analysis, biostatistics, computational analysis): Y.Z. Mazzu, Y. Hu, R.K. Soni, K.M. Mojica, L.-X. Qin, P. Agius, Z.M. Waxman, N.D. Socci, R.C. Hendrickson, T. Tuschl, S. Singer
Writing, review, and/or revision of the manuscript: Y.Z. Mazzu, A. Mihailovic, R.C. Hendrickson, S. Singer
Administrative, technical, or material support (i.e., reporting or organizing data, constructing databases): Y.Z. Mazzu, Y. Hu, K.M. Mojica, A. Mihailovic, T. Tuschl, S. Singer
Study supervision: Y.Z. Mazzu, S. Singer

Acknowledgments

We thank Janet Novak for editing, members of the Singer lab for the help and discussion, and the Antitumor Assessment Core in MSKCC for assistance in mouse experiments.

Grant Support

This study was supported by NIH SPORE in Soft Tissue Sarcoma P50 CA 140146-01 and the NIH/NCI Cancer Center Support Grant P30 CA008748.

The costs of publication of this article were defrayed in part by the payment of page charges. This article must therefore be hereby marked *advertisement* in accordance with 18 U.S.C. Section 1734 solely to indicate this fact.

Received December 5, 2016; revised June 13, 2017; accepted September 1, 2017; published OnlineFirst September 7, 2017.

References

1. Ducimetiere F, Lurkin A, Ranchere-Vince D, Decouvelaere AV, Isaac S, Claret-Tournier C, et al. Incidence rate, epidemiology of sarcoma and molecular biology. Preliminary results from EMS study in the Rhone-Alpes region. Bull Cancer 2010;97:629–41.
2. Brennan MF, Antonescu CR, Moraco N, Singer S. Lessons learned from the study of 10,000 patients with soft tissue sarcoma. Ann Surg 2014;260:416–21; discussion 21–2.
3. Meis-Kindblom JM, Sjogren H, Kindblom LG, Peydro-Mellquist A, Roijer E, Aman P, et al. Cytogenetic and molecular genetic analyses of liposarcoma and its soft tissue simulators: recognition of new variants and differential diagnosis. Virchows Arch 2001;439:141–51.
4. Tan MC, Brennan MF, Kuk D, Agaram NP, Antonescu CR, Qin LX, et al. Histology-based classification predicts pattern of recurrence and improves risk stratification in primary retroperitoneal sarcoma. Ann Surg 2016; 263:593–600.
5. Jones RL, Fisher C, Al-Muderis O, Judson IR. Differential sensitivity of liposarcoma subtypes to chemotherapy. Eur J Cancer 2005;41:2853–60.
6. Krol J, Loedige I, Filipowicz W. The widespread regulation of microRNA biogenesis, function and decay. Nat Rev Genet 2010;11:597–610.
7. Calin GA, Croce CM. MicroRNA signatures in human cancers. Nat Rev Cancer 2006;6:857–66.
8. Vincenzi B, Iuliani M, Zoccoli A, Pantano F, Fioramonti M, De Lisi D, et al. Deregulation of dicer and mir-155 expression in liposarcoma. Oncotarget 2015;6:10586–91.
9. Gits CM, van Kuijk PF, Jonkers MB, Boersma AW, Smid M, van Ijcken WF, et al. MicroRNA expression profiles distinguish liposarcoma subtypes and implicate miR-145 and miR-451 as tumor suppressors. Int J Cancer 2014;135:348–61.
10. Ugras S, Brill E, Jacobsen A, Hafner M, Socci ND, Decarolis PL, et al. Small RNA sequencing and functional characterization reveals microRNA-143 tumor suppressor activity in liposarcoma. Cancer Res 2011;71:5659–69.
11. Borjigin N, Ohno S, Wu W, Tanaka M, Suzuki R, Fujita K, et al. TLS-CHOP represses miR-486 expression, inducing upregulation of a metastasis regulator PAI-1 in human myxoid liposarcoma. Biochem Biophys Res Commun 2012;427:355–60.
12. Bianchini L, Saada E, Gjernes E, Marty M, Haudebourg J, Birtwisle-Peyrottes I, et al. Let-7 microRNA and HMGA2 levels of expression are not inversely linked in adipocytic tumors: analysis of 56 lipomas and liposarcomas with molecular cytogenetic data. Genes Chromosomes Cancer 2011;50: 442–55.
13. Lee DH, Amanat S, Goff C, Weiss LM, Said JW, Doan NB, et al. Over-expression of miR-26a-2 in human liposarcoma is correlated with poor patient survival. Oncogenesis 2013;2:e47.
14. Gimble J, Guilak F. Adipose-derived adult stem cells: isolation, characterization, and differentiation potential. Cytotherapy 2003;5:362–9.
15. Zhang Y, Xie RL, Croce CM, Stein JL, Lian JB, van Wijnen AJ, et al. A program of microRNAs controls osteogenic lineage progression by targeting transcription factor Runx2. Proc Natl Acad Sci U S A 2011;108:9863–8.
16. Wu YV, Okada T, DeCarolis P, Socci N, O'Connor R, Geha RC, et al. Restoration of C/EBPalpha in dedifferentiated liposarcoma induces G_2/M cell cycle arrest and apoptosis. Genes Chromosomes Cancer 2012;51: 313–27.
17. Ramirez-Zacarias JL, Castro-Munozledo F, Kuri-Harcuch W. Quantitation of adipose conversion and triglycerides by staining intracytoplasmic lipids with Oil red O. Histochemistry 1992;97:493–7.
18. Chim CS, Fung TK, Cheung WC, Liang R, Kwong YL. SOCS1 and SHP1 hypermethylation in multiple myeloma: implications for epigenetic activation of the Jak/STAT pathway. Blood 2004;103:4630–5.
19. Majid S, Dar AA, Saini S, Shahryari V, Arora S, Zaman MS, et al. miRNA-34b inhibits prostate cancer through demethylation, active chromatin modifications, and AKT pathways. Clin Cancer Res 2013;19:73–84.
20. Dweep H, Sticht C, Pandey P, Gretz N. miRWalk–database: prediction of possible miRNA binding sites by "walking" the genes of three genomes. J Biomed Inform 2011;44:839–47.
21. Hsu SD, Tseng YT, Shrestha S, Lin YL, Khaleel A, Chou CH, et al. miRTarBase update 2014: an information resource for experimentally validated miRNA-target interactions. Nucleic Acids Res 2014;42:D78–85.
22. Maragkakis M, Vergoulis T, Alexiou P, Reczko M, Plomaritou K, Gousis M, et al. DIANA-microT Web server upgrade supports Fly and Worm miRNA target prediction and bibliographic miRNA to disease association. Nucleic Acids Res 2011;39:W145–8.
23. Wang X.miRDB: a microRNA target prediction and functional annotation database with a wiki interface. RNA 2008;14:1012–7.
24. Betel D, Wilson M, Gabow A, Marks DS, Sander C. The microRNA.org resource: targets and expression. Nucleic Acids Res 2008;36: D149–53.
25. Kruger J, Rehmsmeier M. RNAhybrid: microRNA target prediction easy, fast and flexible. Nucleic Acids Res 2006;34:W451–4.
26. Krek A, Grun D, Poy MN, Wolf R, Rosenberg L, Epstein EJ, et al. Combinatorial microRNA target predictions. Nat Genet 2005;37:495–500.
27. Miranda KC, Huynh T, Tay Y, Ang YS, Tam WL, Thomson AM, et al. A pattern-based method for the identification of MicroRNA binding sites and their corresponding heteroduplexes. Cell 2006;126:1203–17.
28. Agarwal V, Bell GW, Nam JW, Bartel DP. Predicting effective microRNA target sites in mammalian mRNAs. Elife 2015;4:e05005.
29. Kumar S, Fajardo JE, Birge RB, Sriram G. Crk at the quarter century mark: perspectives in signaling and cancer. J Cell Biochem 2014;115: 819–25.
30. Li L, Guris DL, Okura M, Imamoto A. Translocation of CrkL to focal adhesions mediates integrin-induced migration downstream of Src family kinases. Mol Cell Biol 2003;23:2883–92.
31. Mitra SK, Schlaepfer DD. Integrin-regulated FAK-Src signaling in normal and cancer cells. Curr Opin Cell Biol 2006;18:516–23.
32. Marchetti MA, Lee W, Cowell TL, Wells TM, Weissbach H, Kantorow M. Silencing of the methionine sulfoxide reductase A gene results in loss of mitochondrial membrane potential and increased ROS production in human lens cells. Exp Eye Res 2006;83:1281–6.
33. Atashi F, Modarressi A, Pepper MS. The role of reactive oxygen species in mesenchymal stem cell adipogenic and osteogenic differentiation: a review. Stem Cells Dev 2015;24:1150–63.
34. Taylor BS, DeCarolis PL, Angeles CV, Brenet F, Schultz N, Antonescu CR, et al. Frequent alterations and epigenetic silencing of differentiation pathway genes in structurally rearranged liposarcomas. Cancer discovery 2011;1:587–97.

35. Singer S, Socci ND, Ambrosini G, Sambol E, Decarolis P, Wu Y, et al. Gene expression profiling of liposarcoma identifies distinct biological types/subtypes and potential therapeutic targets in well-differentiated and dedifferentiated liposarcoma. Cancer Res 2007;67:6626–36.
36. Wang J, Chen X, Li P, Su L, Yu B, Cai Q, et al. CRKL promotes cell proliferation in gastric cancer and is negatively regulated by miR-126. Chem Biol Interact 2013;206:230–8.
37. Tamura M, Sasaki Y, Kobashi K, Takeda K, Nakagaki T, Idogawa M, et al. CRKL oncogene is downregulated by p53 through miR-200s. Cancer Sci 2015;106:1033–40.
38. Chiarugi P, Pani G, Giannoni E, Taddei L, Colavitti R, Raugei G, et al. Reactive oxygen species as essential mediators of cell adhesion: the oxidative inhibition of a FAK tyrosine phosphatase is required for cell adhesion. J Cell Biol 2003;161:933–44.
39. Mian MF, Kang C, Lee S, Choi JH, Bae SS, Kim SH, et al. Cleavage of focal adhesion kinase is an early marker and modulator of oxidative stress-induced apoptosis. Chem Biol Interact 2008;171:57–66.
40. Li JJ, Xie D. Cleavage of focal adhesion kinase (FAK) is essential in adipocyte differentiation. Biochem Biophys Res Commun 2007;357:648–54.
41. Du Y, Liu Z, Gu L, Zhou J, Zhu BD, Ji J, et al. Characterization of human gastric carcinoma-related methylation of 9 miR CpG islands and repression of their expressions in vitro and in vivo. BMC Cancer 2012;12:249.
42. Rauhala HE, Jalava SE, Isotalo J, Bracken H, Lehmusvaara S, Tammela TL, et al. miR-193b is an epigenetically regulated putative tumor suppressor in prostate cancer. Int J Cancer 2010;127:1363–72.
43. Londono Gentile T, Lu C, Lodato PM, Tse S, Olejniczak SH, Witze ES, et al. DNMT1 is regulated by ATP-citrate lyase and maintains methylation patterns during adipocyte differentiation. Mol Cell Biol 2013;33:3864–78.